Dysferlin stabilizes stress-induced Ca^{2+} signaling in the transverse tubule membrane

Jaclyn P. Kerr[a,1], Andrew P. Ziman[a,1], Amber L. Mueller[a], Joaquin M. Muriel[a], Emily Kleinhans-Welte[a], Jessica D. Gumerson[a], Steven S. Vogel[b], Christopher W. Ward[c], Joseph A. Roche[a], and Robert J. Bloch[a,2]

[a]Department of Physiology, University of Maryland School of Medicine, Baltimore, MD 21201; [b]Section on Cellular Biophotonics, Laboratory of Molecular Physiology, National Institute on Alcohol Abuse and Alcoholism, National Institutes of Health, Bethesda, MD 20892-9411; and [c]University of Maryland School of Nursing, Baltimore, MD 21201

Edited* by Louis M. Kunkel, Children's Hospital Boston, Harvard Medical School, Boston, MA, and approved November 12, 2013 (received for review April 29, 2013)

Dysferlinopathies, most commonly limb girdle muscular dystrophy 2B and Miyoshi myopathy, are degenerative myopathies caused by mutations in the *DYSF* gene encoding the protein dysferlin. Studies of dysferlin have focused on its role in the repair of the sarcolemma of skeletal muscle, but dysferlin's association with calcium (Ca^{2+}) signaling proteins in the transverse (t-) tubules suggests additional roles. Here, we reveal that dysferlin is enriched in the t-tubule membrane of mature skeletal muscle fibers. Following experimental membrane stress in vitro, dysferlin-deficient muscle fibers undergo extensive functional and structural disruption of the t-tubules that is ameliorated by reducing external [Ca^{2+}] or blocking L-type Ca^{2+} channels with diltiazem. Furthermore, we demonstrate that diltiazem treatment of dysferlin-deficient mice significantly reduces eccentric contraction-induced t-tubule damage, inflammation, and necrosis, which resulted in a concomitant increase in postinjury functional recovery. Our discovery of dysferlin as a t-tubule protein that stabilizes stress-induced Ca^{2+} signaling offers a therapeutic avenue for limb girdle muscular dystrophy 2B and Miyoshi myopathy patients.

excitation–contraction coupling | dihydropyridine receptor | triad junction | muscle injury

Dysferlinopathies are degenerative myopathies secondary to mutations in the gene encoding the protein dysferlin. These myopathies, most commonly limb girdle muscular dystrophy type 2B (LGMD2B) and Miyoshi myopathy (MM), are independent of motor neuron activation (1), indicating that they are myogenic in origin. Dysferlin is a 230-kDa protein composed of seven C2 domains with homology to synaptotagmin (2, 3) and a single transmembrane domain near its C terminus (4, 5). The complexity of dysferlin's potential role in muscle is highlighted by the number of its purported functions, including membrane repair (2, 3), vesicle fusion (4), microtubule regulation (5, 6), cell adhesion (7, 8), and intercellular signaling (9). Understanding the contributions of dysferlin to the maintenance of normal skeletal muscle function is critical for the development of appropriate therapies for patients diagnosed with LGMD2B and MM.

Recently, we demonstrated the localization of dysferlin at the A-I junction in mature muscle fibers (10). These results agree with earlier reports associating dysferlin with the dihydropyridine receptor (DHPR, L-type Ca^{2+} channel), Ahnak, caveolin 3, and several other proteins involved in Ca^{2+}-based signaling and the function of transverse (t-) tubules (11–14). Consistent with this localization and the potential for a functional role in this specialized compartment, dysferlin-deficient murine muscle demonstrates altered transverse tubule (t-tubule) structure (15) as well as increased oxidative stress (16, 17), inflammation, and necrosis (18–20) after injury.

Here we demonstrate that dysferlin is enriched in the t-tubule membrane, where it contributes to the maintenance of the t-tubule and Ca^{2+} homeostasis. We show that, although the structure and function of dysferlin-deficient t-tubules are normal at rest, they are more readily disrupted following experimental injury and are protected by reducing extracellular [Ca^{2+}] or blocking L-type Ca^{2+} channels with diltiazem. We also demonstrate that treatment of dysferlin-deficient mice with diltiazem significantly improves their recovery from injuries induced by eccentric contractions. These findings support a role for dysferlin in stabilizing the t-tubules of skeletal muscle subjected to stress and suggest that diltiazem treatment may represent a viable therapeutic option for LGMD2B and MM patients.

Results

Our first experiments were directed at determining the subcellular localization of dysferlin in mature skeletal muscle fibers. Isolated adult myofibers from the flexor digitorum brevis (FDB) muscles of control mice were immunostained for dysferlin and DHPR to assess their colocalization (Fig. 1*A* and Fig. S1). Both proteins localized in a doublet pattern, consistent with the t-tubule localization of DHPR. Analysis by Mander's coefficient of colocalization indicated that ~47% of the DHPR colocalized with dysferlin ($n = 8$; 0.475 ± 0.016 SEM). We found similar colocalization between the ryanodine receptor (RyR) and dysferlin ($n = 4$; 0.482 ± 0.022 SEM) (Fig. S1), suggesting that endogenous dysferlin localizes at or near the triad junction. Dysferlin also closely localized with other t-tubule–associated proteins, such as Bin1, junctophilin, and caveolin 3 (Cav3), but it was not enriched in sarcolemmal structures that stained brightly for Cav3 (Fig. S1). Expression of exogenous Venus-dysferlin in control FDB fibers also resulted in a prominent doublet pattern that colocalized with the lipophilic dye, di-8-ANEPPS (Fig. 1*B*). Together,

Significance

Muscular dystrophies linked to the genetic absence or mutations of dysferlin are currently without a relevant therapy. Dysferlin is thought to mediate membrane repair in skeletal muscle, but its localization and specific functions remain controversial. Here we show that dysferlin is enriched in the transverse tubule membrane of skeletal muscle and demonstrate that, in its absence, mechanical stress leads to calcium-dependent muscle injury. Furthermore, we demonstrate that treatment of dysferlin-deficient muscle with the calcium channel blocker diltiazem reduces in vitro experimental and in vivo contraction-induced muscle damage. As diltiazem is approved for clinical use, our results suggest a potential new therapeutic avenue for patients diagnosed with dysferlinopathies.

Author contributions: J.P.K., A.P.Z., C.W.W., J.A.R., and R.J.B. designed research; J.P.K., A.P.Z., A.L.M., J.M.M., E.K.-W., J.D.G., C.W.W., and J.A.R. performed research; J.M.M., E.K.-W., and S.S.V. contributed new reagents/analytic tools; J.P.K., A.P.Z., A.L.M., J.D.G., C.W.W., and J.A.R. analyzed data; and J.P.K. and R.J.B. wrote the paper.

The authors declare no conflict of interest.

*This Direct Submission article had a prearranged editor.

[1]J.P.K. and A.P.Z. contributed equally to this work.

[2]To whom correspondence should be addressed. E-mail: rbloch@umaryland.edu.

This article contains supporting information online at www.pnas.org/lookup/suppl/doi:10.1073/pnas.1307960110/-/DCSupplemental.

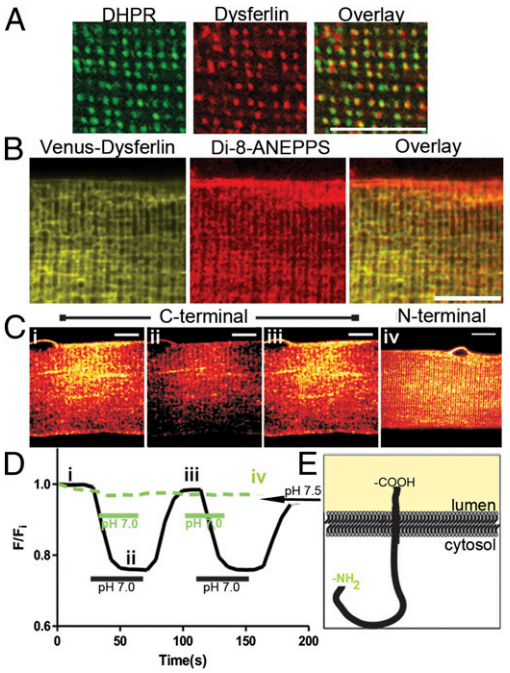

Fig. 1. Dysferlin is a t-tubule protein. (*A*) Double-immunofluorescence labeling shows colabeling of dysferlin with DHPR. Analysis with Mander's coefficient shows that ~47% of DHPR colocalizes with dysferlin (M1 = 0.475 ± 0.016 SEM; n = 8). (*B*) FDB fibers were electroporated with cDNA plasmid encoding Venus-tagged dysferlin. Isolated fibers were treated with the lipophilic dye, di-8-ANEPPS. Venus-dysferlin colocalized with di-8-ANEPPS at the t-tubule doublets, but to a lesser extent at the sarcolemma. (*C*) FDB fibers overexpressing fusion proteins of pHluorin and dysferlin. Dysferlin with pHluorin at both the C terminus (i–iii) and N terminus (iv) show localization to doublets. (*D*) C-terminal pHluorin-dysferlin (black trace, i–iii in *D*) responds to changes in extracellular pH (~25% decrease in fluorescence from pH 7.5 to pH 7.0); no significant change with the N-terminal pHluorin (green trace) was apparent. (*E*) A schematic representation of dysferlin shows the orientation of the protein in the t-tubule membrane. (Scale bars, 10 μm.)

these data indicate a preferential association of dysferlin with components of t-tubules and triad junctions.

To determine if dysferlin was localized within the t-tubule membrane, rather than in the junctional SR membrane or in cytosolic structures associated with the t-tubule, we exogenously expressed dysferlin with a pH-sensitive GFP (pHluorin) (21) fused to either its C or N terminus. Expression of each pHluorin-dysferlin construct (Fig. 1*C*) resulted in a pattern of distribution similar to both endogenous dysferlin (cf. Fig. 1*A*) and exogenously expressed Venus-dysferlin (cf. Fig. 1*B*). Decreasing the pH of the extracellular medium from pH 7.5 to pH 7.0 reduced the fluorescence intensity of the C-terminal pHluorin-dysferlin (Fig. 1 *C* and *D*, black line), indicating that the pHluorin moiety, and by extension the C terminus of dysferlin, was exposed to the lumen of the t-tubule. As the N-terminal pHluorin-dysferlin did not respond to changes in extracellular pH (Fig. 1 *C* and *D*, green line), we conclude that dysferlin associates with the t-tubule membrane and that it is oriented with its C terminus exposed to the extracellular space (Fig. 1*E*). This localization for dysferlin led us to hypothesize that dysferlin contributes to the function of the t-tubule.

As dysferlin-deficient muscle exhibits increased t-tubule damage (15), we modified an osmotic shock injury (OSI) assay, demonstrated to detect t-tubule defects in dystrophic models (22–24), and used a cell-impermeant dye (Sulforhodamine B, or SulfB) to assess the changes in dye efflux from the t-tubule caused by acute OSI (Fig. 2*A*). Following perfusion with isotonic Tyrode's + SulfB to fill the t-tubule lumen, a switch to isotonic Tyrode's initiated a decrease in SulfB fluorescence, and the kinetics of this decrease was taken as a measure of the mobility of molecules within the t-tubule space. Uninjured AJ (dysferlin-null) and WT fibers demonstrated equivalent kinetics before OSI. After OSI, t-tubule dye clearance of both experimental groups was slowed, but it was significantly slower in dysferlin-null fibers (Fig. 2 *B* and *D*). This impaired dye clearance in dysferlin-null myofibers was associated with residual dye trapped in the t-tubule, evidenced by dye-filled structures 10 min post-OSI (Fig. 2*A*, *Center*).

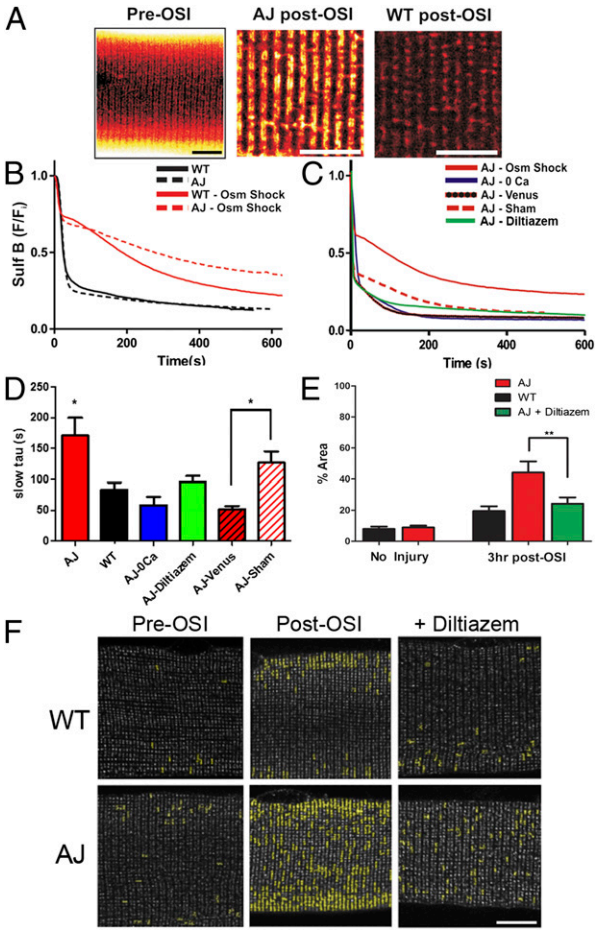

Fig. 2. Dysferlin-null myofibers are more susceptible to t-tubule damage in vitro. (*A*) SulfB revealed that the overall organization of the t-tubule does not differ significantly between AJ and WT (*Left*). Following OSI, a large amount of SulfB remains in the AJ t-tubules (*Center*) but not in WT (*Right*). (*B*) The kinetics of efflux of SulfB from t-tubules during washout (black lines) before OSI are indistinguishable between dysferlin-null and controls. Following osmotic shock, the mobility of SulfB was greatly reduced in AJ fibers (red dashed line) compared with WT controls (red solid line). (*C*) Dysferlin-null expressing Venus-dysferlin were resistant to osmotic shock (red line and black dashed line; AJ-Venus) compared with sham-transfected fibers (dashed red line; AJ-sham). In AJ fibers, removal of extracellular Ca^{2+} (blue line) or pretreatment (30 min) with diltiazem (green line) normalized dye clearance to near control rates. (*D*) Pooled data for the time constants (tau) of the slower phase of dye release under the different conditions assayed. (*E* and *F*) Dysferlin-null and WT FDB fibers immunolabeled for DHPR (grayscale; see also Fig. S2). The images were analyzed to assess areas of clustered DHPR (shown in yellow highlights) following OSI. Pooled data (*E*) show that only 10–15% of the area in uninjured dysferlin-null or control fibers is disrupted. Clustering of DHPR in dysferlin-null fibers increased to 44% at 3 h post-OSI. Treatment with diltiazem before and during osmotic shock decreased DHPR disruption in injured dysferlin-null fibers to levels indistinguishable from controls. We found no change in dysferlin distribution following OSI in WT FDB fibers (Fig. S2*C*). (Scale bars, 10 μm.) $*P < 0.05$, $**P < 0.01$.

We confirmed the role of dysferlin in this process by expressing full-length dysferlin in dysferlin-null FDB fibers and by demonstrating SulfB washout kinetics similar to controls (Fig. 2 *C* and *D*). As the reintroduction of dysferlin into dysferlin-null FDB fibers was sufficient to protect them from OSI-induced pathology, we consider this to be a robust assay of dysferlin's role in maintaining the t-tubule following experimental stress.

The effect of OSI on dysferlin-null t-tubules was further assessed by examining the organization of the DHPR. Before OSI, immunostained DHPR appeared as discrete puncta (~0.1 μm^2) in both control and dysferlin-null fibers (Fig. 2*F* and Fig. S2). Furthermore, areas of DHPR aggregation and clustering (>0.4 μm^2; Fig. 2*F*, yellow overlay) were rare, as they occupied less than 10% of the total DHPR area (Fig. 2*E*). Following OSI, DHPR clustering was significantly increased in dysferlin-deficient myofibers (44% total DHPR area) compared with WT (20%).

It is well established that Ca^{2+} influx contributes to OSI-induced muscle injury (23, 25, 26). In dysferlin-null FDB fibers, removal of extracellular $[Ca^{2}]^{+}$ ablated OSI-induced deficits in SulfB dye clearance (Fig. 2 *C* and *D*), which implicates Ca^{2+}-dependent processes in the t-tubule disruption. As OSI activates DHPR Ca^{2+} influx (25) and dysferlin interacts with the DHPR (10), we tested the hypothesis that DHPR Ca^{2+} influx underscored the enhanced OSI-induced t-tubule damage in dysferlin-null myofibers. Pretreatment with diltiazem (an L-type Ca^{2+} channel blocker) prevented the OSI-induced deficits in SulfB dye clearance (Fig. 2 *C* and *D*), as well as the aggregation of DHPR (Fig. 2 *E* and *F* and Fig. S2). We found no difference in DHPR expression between genotypes (Fig. S3), supporting DHPR function, not expression level, as a contributing factor to the OSI effect in dysferlin-null fibers. These results support a role for dysregulated Ca^{2+} influx in enhanced t-tubule sensitivity to OSI in dysferlin-null myofibers.

These effects were model-independent, as we obtained similar results with myofibers from the BlaJ mouse model of dysferlinopathy. As the BlaJ mouse demonstrates a more rapid progression of muscle degeneration than the AJ model (18, 27), we opted to use mice at 2 mo of age, before the reported onset of myopathy, to test the effects of the absence of dysferlin on the sensitivity of the BlaJ myofibers to OSI and on the protective action of diltiazem. Using a similar image analysis strategy to that used in the AJ, we found that BlaJ fibers exhibit significantly more DHPR clustering (DHPR clusters >0.4 μm^2) post-OSI than the control (C57/Bl6) ($P < 0.05$) and that diltiazem blocked this increase (Fig. S4).

Next we sought to determine whether DHPR function was intrinsically altered or if the differences seen in dysferlin-null myofibers manifested only with OSI. In dysferlin-null myofibers equilibrated with the ratiometric Ca^{2+} dye, Indo-1, no differences in resting cytosolic $[Ca^{2+}]$ or in the amplitude of electrically evoked Ca^{2+} transients were seen (Fig. S5). The effect of OSI on DHPR function was assessed in Fluo-4–loaded dysferlin-null myofibers (Fig. 3), stimulated at 1 Hz for 10 s before OSI and again each minute following OSI for a total of 5 min. Post-OSI, a significant impairment in the amplitude of Ca^{2+} transients (75% decrease) (Fig. 3 *A* and *B*) was accompanied by a progressive rise in cytosolic $[Ca^{2+}]$ in dysferlin-null myofibers (Fig. 3 *A* and *C*). Diltiazem treatment protected the dysferlin-null fibers from the OSI-induced impairment in transient amplitude (Fig. 3 *A* and *B*) while also preventing the increase in cytosolic Ca^{2+} ($P < 0.01$) (Fig. 3 *A* and *C*). These results support a model in which dysferlin contributes to the protection of the t-tubule from stress caused by OSI by maintaining normal Ca^{2+} signaling. Furthermore, the effectiveness of diltiazem implicates the L-type Ca^{2+} channel, rather than membrane disruption, as the pathway for Ca^{2+} influx in dysferlinopathy.

Dysferlinopathies are associated with increased myofiber necrosis and enhanced immune and inflammatory responses, gauged by increased monocyte and macrophage infiltration (28, 29). Previously, we reported that impaired recovery of contractile

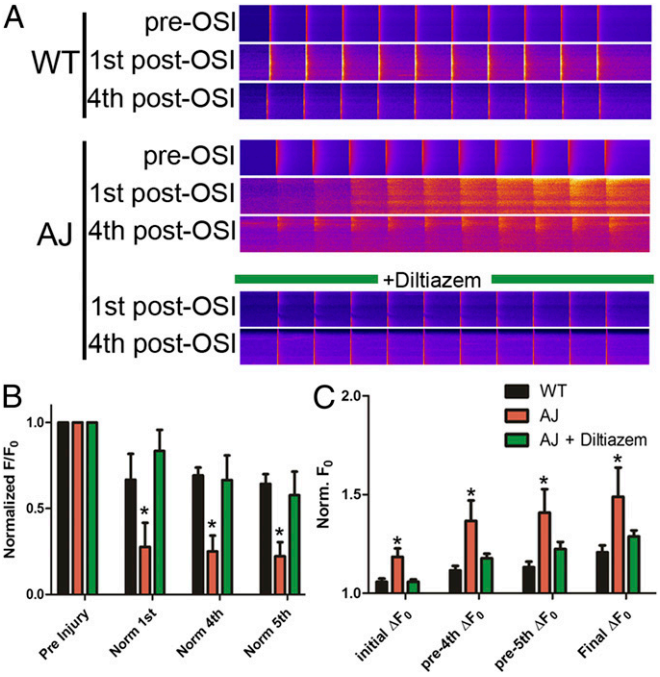

Fig. 3. Dysferlin-null myofibers exhibit altered Ca^{2+} regulation following injury. (*A*) Representative linescans of Ca^{2+} transients derived from WT (*Top*) and AJ (*Middle*) myofibers before OSI ("pre-OSI" rows), obtained with fibers loaded with Fluo-4, demonstrate normal Ca^{2+} homeostasis. Following OSI ("1st post-OSI" and "4th post-OSI" rows), both WT and AJ myofibers exhibit altered Ca^{2+} homeostasis, with the AJ myofibers demonstrating increased cytosolic Ca^{2+} and depressed transients. Diltiazem treatment (*Bottom*) largely prevents these changes in the AJ myofibers following OSI, resulting in transients that closely resemble WT. (*B*) Pooled normalized data demonstrate that the amplitudes of Ca^{2+} transients in dysferlin-null (AJ) fibers are significantly reduced from their preinjury levels following osmotic shock. Following diltiazem treatment, Ca^{2+} transients in dysferlin-null myofibers are maintained. (*C*) Basal cytosolic Ca^{2+} is elevated in dysferlin-null fibers after osmotic shock and continues to rise at a greater rate than controls. Cytosolic Ca^{2+}in diltiazem-treated dysferlin-null myofibers is similar to controls. *$P < 0.05$.

torque following large-strain injury (LSI) in dysferlin-null mice was concurrent with an increase in necrosis and macrophage infiltration (19). As diltiazem protected dysferlin-null myofibers from injury by osmotic shock in vitro, we tested whether systemic treatment of dysferlin-null mice with diltiazem improved the response of muscle injured by LSI in vivo.

We subjected control and dysferlin-deficient mice to LSI of the hind-limb ankle dorsiflexor muscles and assessed the effect of diltiazem treatment on the phenotypic changes in the tibialis anterior (TA) muscle. LSI caused significant disruption of DHPR in dysferlin-null but not in control muscle at 3 h post-injury (Fig. 4*A*). Systemic treatment of dysferlin-null mice with diltiazem significantly decreased the number of injured fibers with disrupted DHPR ($P < 0.001$). Although diltiazem had no effect on the extent of the injury immediately after LSI (Fig. 4*B* and Fig. S6), it promoted better recovery of contractile torque 3 d after injury (Fig. 4*B*). Consistent with this result, diltiazem also reduced the number of necrotic myofibers and in-flammatory macrophages at 3 d post-LSI (Fig. 4 *C* and *D* and Fig. S7), as well as the number of centrally nucleated fibers at 14 d post-LSI (Fig. 4*E*) ($P < 0.01$). This enhanced recovery with diltiazem treatment occurred without changes in the protein expression of DHPR, RyR, or other t-tubule–associated proteins (Figs. S8 and S9). These studies demonstrate that diltiazem's inhibition of Ca^{2+} influx through the DHPR protects dysferlin-null myofibers from stress-induced t-tubule disruption and reduces the amount of fiber death, inflammation, and regeneration associated with the

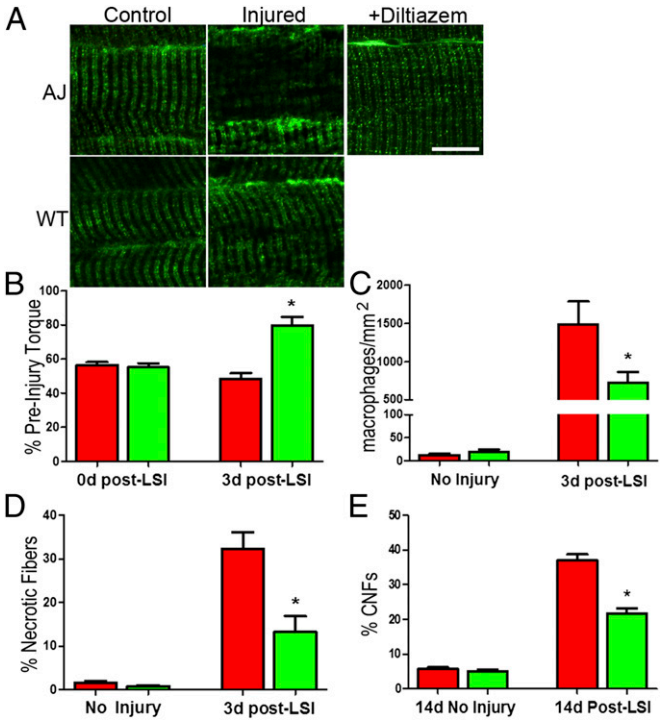

Fig. 4. Diltiazem treatment protects dysferlin-null muscle in vivo. (*A*) Following LSI, disruptions in DHPR immunostaining are evident as areas showing a decrease and disruption of DHPR labeling in AJ muscle. Systemic diltiazem largely inhibits the increase in disruption following LSI in AJ muscle fibers, decreasing it from 58 to 12% ($P < 0.001$). Following LSI injury, only 5.7% of myofibers in WT muscle showed disrupted DHPR organization. (Fig. S7). (*B*) In vivo treatment of dysferlin-null mice with diltiazem significantly improves the recovery of torque 3 d after LSI. (*C*) Diltiazem treatment significantly reduces the number of inflammatory cells in dysferlin-null muscle at 3 d post-LSI. (*D*) Treatment with diltiazem significantly reduces the number of necrotic fibers in dysferlin-null muscle at 3 d post-LSI. (*E*) Diltiazem treatment significantly reduced the number of centrally nucleated fibers (CNFs) in dysferlin-null muscle at 14 d post-LSI. (Scale bars, 10 μm.) $*P < 0.05$, $**P < 0.001$.

recovery of dysferlin-null muscle after eccentric injury (cf. 19). They therefore support our hypothesis that the susceptibility of dysferlin-null muscle to injury results from a Ca^{2+}-dependent destabilization of t-tubules and that blocking excessive Ca^{2+} entry with diltiazem ameliorates the downstream pathology.

Discussion

Here we demonstrate that dysferlin is an integral protein of the t-tubule membrane that stabilizes stress-induced Ca^{2+} signaling in the t-tubule membrane. These conclusions are supported by our localization of dysferlin to the t-tubule and our demonstration that dysferlin-null myofibers exhibit Ca^{2+}-dependent structural damage to t-tubules following injury. The effectiveness of diltiazem, a drug that inhibits the influx of Ca^{2+} through the DHPR, in preventing structural and functional changes in t-tubules implicates this pathway as a potential therapeutic target in dysferlinopathy.

Although originally identified as a protein of the sarcolemma (3, 30, 31), dysferlin has also been shown to be present in the interior of myofibers, particularly in dystrophic muscle (10, 32, 33). Dysferlin was also found to coimmunoprecipitate with DHPR from developing myotubes and was hypothesized to be important for the development of the t-tubule (11, 15). Other studies found dysferlin at the level of the A-I junction of stretched muscle (14), and we previously localized dysferlin to that region in mature muscle (10). Our current data (cf. Fig. 1 *C*–*E*) specifically place dysferlin in the membrane of the t-tubule in mature myofibers, with its C terminus exposed to the lumen. This finding, combined with our demonstrations that dysferlin is present at triad junctions (Fig. 1*A* and Fig. S1) and that t-tubules and Ca^{2+} homeostasis are unstable in stressed muscle when dysferlin is absent (Figs. 2–4), suggest the hypothesis that dysferlin interacts with DHPR and contributes to the maintenance of t-tubule function and Ca^{2+} homeostasis.

Our proposed role for dysferlin is an addition to the current view of dysferlin as a sarcolemmal repair protein. Much of the data leading to the membrane repair hypothesis was gathered using myoblasts or immature myotubes (34, 35), in which the intracellular membrane systems typical of adult skeletal muscle, such as the t-tubules, are either absent or in an immature state. Thus, these model systems may not fully represent the role of dysferlin in mature myofibers. Studies performed in mature muscle have relied on electron microscopy of dysferlinopathic muscle and on laser wounding to study dysferlin and its function as a sarcolemmal repair protein (2, 3, 36–38). However, the ability of laser wounding to predict the outcome of interventional treatments for dysferlinopathies has been recently questioned (39). Furthermore, recent evidence suggests that dysferlin, although recruited to the wounded sarcolemma (3), is not necessary for the immediate resealing of the damaged sarcolemmal membrane following laser wounding (40, 41) or large-strain lengthening contractions (20).

Our results suggest that dysferlin is required for the maintenance of functional t-tubules and that a deficiency in dysferlin leads to Ca^{2+}-dependent alterations in t-tubule morphology and function. Our demonstration that the expression of exogenous dysferlin in dysferlin-null myofibers is sufficient to protect against stress-induced damage in vitro directly implicates dysferlin as a causal factor. Furthermore, our ability to prevent injury by removing extracellular Ca^{2+} or by blocking Ca^{2+} entry with diltiazem implicates the proximate involvement of the DHPR/L-type Ca^{2+} channel in the dysferlinopathic process, rather than mechanically induced sarcolemmal tears (9). However, recent evidence linking DHPR activation to other Ca^{2+} permeation pathways (e.g., Orai1 or a TRP channel) (42) does not allow us to rule out the contribution of additional influx pathways to the degradation of t-tubule function following stress.

The effectiveness of diltiazem at preventing the in vitro pathology and stress-induced Ca^{2+} signaling led us to study whether systemic treatment of dysferlin-null mice would promote recovery from large-strain eccentric injury. Short-term treatment with diltiazem before in vivo injury significantly decreased the number of fibers displaying disrupted DHPR morphology shortly after LSI and significantly increased recovery of torque 3 d later. As previously reported, the downstream consequences of LSI in dysferlin-deficient muscle include considerable necrosis and inflammation, followed by muscle regeneration (18–20). Diltiazem treatment decreased the number of necrotic fibers and the severity of the inflammatory response 3 d after physiological injury and decreased the number of centrally nucleated fibers 14 d after injury. We speculate that, by acting on the DHPR, diltiazem reduced the increase in cytoplasmic $[Ca^{2+}]$ after injury and thus prevented the activation of Ca^{2+}-mediated processes, such as calpain activation and mitochondrial damage, which can promote secondary damage and necrosis. These results further indicate that the pathology of dysferlin deficiency can be mitigated by targeting this pathway.

Here we reveal a role for dysferlin as a stabilizer of Ca^{2+} homeostasis and t-tubule function during membrane stress. Taken with the discovery of dysferlin as an integral t-tubule membrane protein, our data support t-tubule Ca^{2+} dysregulation as an avenue for therapeutic interventions. Because diltiazem, an FDA-approved drug, significantly protects dysferlin-deficient muscle from injury, we suggest that it should be considered as a potential intervention to slow the continued progression of dysferlinopathies in patients with LGMD2B and MM.

Materials and Methods

Mice. Dysferlin-null (AJ or BlaJ) and control A/WynSnJ and C57BL/6 (WT) mice were obtained either directly from the Jackson Laboratory or from breeding colonies maintained at the University of Maryland, Baltimore. AJ and A/WynSnJ mice used for this study were 12–16 wk of age; BlaJ and C57BL/6 mice were 8 wk of age. All experimental protocols involving animals were approved by the Institutional Animal Care and Use Committee of the University of Maryland School of Medicine.

In Vivo Experimentation. In vivo measurements of torque and large-strain injury of the hind-limb ankle dorsiflexor muscle group were performed as described (19, 43). Briefly, injury was induced by a series of 20 lengthening contractions performed by stretching the tetanically stimulated left-ankle dorsiflexors through an arc of 90°–180° of plantarflexion at 1,200°/sec. Contractile torque was measured before, immediately after, and 3 d after injury to assess susceptibility to injury and recovery thereafter. As the TA muscle accounts for ∼90% of the force generated by the ankle dorsiflexors (44), we used this muscle for all our histological studies.

Immunofluorescence of TA Muscle. We followed the protocols in Roche et al. (10). Animals were perfusion-fixed with ice-cold 4% (wt/vol) paraformaldehyde in PBS. TA muscles were snap-frozen in a liquid nitrogen slurry, cut longitudinally (16 μm), and mounted on glass slides. Sections were labeled with primary antibodies to DHPR (mouse, MA3-920; Thermo Scientific) and dysferlin (rabbit, Romeo 5140–1; Epitomics) followed by labeling with species-specific secondary antibodies conjugated to either AlexaFluor488 or AlexaFluor568 (Invitrogen). Samples were observed under confocal optics with a Zeiss 510 confocal microscope (63×/1.4 N.A. Plan-Apo objective; Carl Zeiss, Inc.).

Isolation of Myofibers from FDB Muscle. Mice were anesthetized and FDB muscles were harvested bilaterally. Single myofibers were enzymatically isolated in DMEM with 2% (wt/vol) BSA, 1 μL/mL gentamicin, and 2 mg/mL type II collagenase (Gibco, Life Technologies) for 2 h at 37 °C, as adapted from ref. 45. Myofibers were incubated at 37 °C for 12–24 h and plated on glass coverslips coated with Matrigel (BD Biosciences) or Geltrex (Invitrogen) before experimentation.

For experiments involving treatment with diltiazem, isolated myofibers were treated with 10 μM diltiazem for 30 min at 37 °C before osmotic shock and experimentation.

Immunofluorescence of FDB Fibers. Myofibers from FDB muscles, cultured as above, were fixed at room temperature for 15 min with 4% electron microscopy (EM)-grade formaldehyde in PBS. Cells were permeabilized in 0.1% Triton X-100 in PBS for 8 min, washed, and incubated with SuperblockPBS (Thermo Scientific) for 2 h at room temperature. Coverslips were incubated in primary antibody overnight at 4 °C and in secondary antibodies for 4 h at room temperature. All primary and secondary antibodies were diluted in SuperblockPBS. Primary antibodies included mouse anti-DHPRα1, rabbit anti-dysferlin, and mouse anti-RyR1 (clone R129; Sigma Aldrich). Secondary antibodies and observation of samples under confocal optics were as above. Colocalization was assessed using Mander's coefficients with ImageJ and the Just Another Colocalization Plugin (46) and reported as M1 (overlap between DHPR or RyR and dysferlin). Other antibodies used for immunofluorescence include Bin1 (EMD Millipore), caveolin 3 (BD Biosciences), junctophilin-1 (Invitrogen), junctophilin-2 (Invitrogen), and mouse anti-dysferlin ("Hamlet"; Leica Biosystems).

Plasmid Constructs. mVenus-dysferlin (N-terminal Venus) (9) (Addgene plasmid 29768) was provided by The Jain Foundation (www.jain-foundation.org). N-terminal pHluorin-dysferlin was constructed by S. V. Koushik (BDRA Consulting, LLC, Damascus, MD), in the S.S.V. laboratory by replacing the Venus ORF from mVenus-dysferlin with the ORF of pHluorin using standard molecular biological techniques. C-terminal pHluorin-dysferlin was generated by excising the Venus tag from the mVenus-dysferlin plasmid, described above, using AgeI and EcoRI restriction enzymes. The pHluorin tag was amplified via PCR from the N-terminal pHluorin-dysferlin construct, using primers to introduce AgeI and EcoRI restriction sites into the tag. The dysferlin plasmid was then ligated to the pHluorin tag and sequenced.

In vivo gene transfer via electroporation into FDB fibers was adapted from published methods (47). Further details are provided in *SI Materials and Methods*.

pHluorin Assay. FDB fibers from control mice were electroporated with a plasmid encoding dysferlin tagged with pH-sensitive GFP (pHluorin) linked to either the C or N terminus. Fibers expressing the pHluorin-dysferlin constructs were studied under confocal optics with a Zeiss LSM510 microscope (40×/1.4 N.A. Plan-Apo objective). During imaging, pHluorin-positive cells were perfused with buffered saline (pH 7.5). At regular intervals, the perfusate was switched to a solution at pH 7.0.

Sulforhodamine B Clearance. Cultured FDB fibers were superfused with 50 μM SulfB, a cell-impermeant dye, in normal Tyrode's solution (140 mM NaCl, 0.5 mM $MgCl_2$, 0.3 mM NaH_2PO_4, 5 mM Hepes, 5.5 mM glucose, 1.8 mM $CaCl_2$, 5 mM KCl_2, pH 7.4) for 30 s (SulfB/Tyrode's, adapted from ref. 48). Cells were then perfused with a hypotonic (Tyrode's solution containing half the normal concentration of NaCl) SulfB/Tyrode's solution to induce swelling. After 30 s, cells were perfused with isotonic SulfB/Tyrode's solution and then perfused with dye-free isotonic Tyrode's solution. Dye washout was recorded by confocal microscopy for 10 min following OSI. Ca^{2+}-free solutions contained 1 mM EGTA and no added Ca^{2+}.

Osmotic Shock Injury. Cultured FDB fibers were superfused with normal Tyrode's solution and then perfused with a hypotonic Tyrode's solution in which the NaCl concentration was decreased to 70 mM for 30 s to induce swelling. Cells were then perfused with isotonic Tyrode's solution and allowed to recover.

Recording of Ca^{2+} Transients. Indo-1 transients were recorded from AJ and control FDB fibers as previously described (49, 50). Further details are provided in *SI Materials and Methods*.

To record changes in cytosolic Ca^{2+} and Ca^{2+} transients induced by OSI, cultured FDB fibers were incubated with 10 μM fluo-4AM (solubilized in 15% pluronic/DMSO) for 30 min at room temperature and imaged with a Zeiss LSM510 (40×/1.4 N.A. Plan-Apo objective) in linescan mode. Contraction was prevented with 50 μM *N*-benzyl-*p*-toluene sulfonamide. Cells were washed in normal Tyrode's, and Ca^{2+} transients were induced by field stimulation (1 Hz for 10 s). Following the recording of initial Ca^{2+} transients, the cells were subjected to hypoosmotic shock, as above. Ca^{2+} transients were then recorded (1 Hz for 10 s) every 1 min for 5 min. Data were collected from the resulting linescan images using ImageJ.

Analysis of T-Tubule Disruption. Disruption of DHPR labeling at the t-tubules of isolated FDB fibers was assessed using Volocity software (PerkinElmer) on immunofluorescence images of DHPR. To assess total t-tubule area, fluorescence signals ≥0.1 μm^2 in area were identified and their area was calculated. These signals were compared with the area calculated from fluorescent signals >0.4 μm^2 in area, generating a percentage area occupied by DHPR labeling that was disrupted. Ten images from each treatment were analyzed.

For in vivo assessments, we followed immunolabeling protocols similar to those used in ref. 10. Disruption of t-tubules was quantified by counting the number of fibers that showed disrupted DHPR labeling and expressing it as a percentage of the total number of fibers counted in each visual field. A total of 70–90 fibers across six visual fields were studied per injured and control TA from each animal.

Diltiazem Administration to Animals. Diltiazem was administered by i.p. injection at a dosage of 72 mg/kg/d (51). The drug was dissolved in PBS (pH 7.4) at 72 mg/10 mL, and 100 μL of this mixture was administered per 10 g body weight. Animals were preconditioned for 7 d before LSI, as our pilot experiments showed that they do not tolerate anesthesia well without preconditioning. On the day of LSI, animals were administered 50% of the daily dose ∼30 min before injury and 50% of the dose immediately after injury. For animals that were studied 3 d and 14 d after LSI, once daily dosing was continued until the time of assay. A sham treatment group received only PBS, according to the same injection regimen.

Assessment of Myofiber Damage and Macrophage Infiltration. To count necrotic myofibers, frozen cross-sections (8 μm) of the injured (left) and uninjured (right) TA muscles were stained with hematoxylin and eosin (H&E), as described (19). The percentage of necrotic myofibers in each muscle was calculated by taking the average across 12 unique fields (20× objective lens, Zeiss Axioskop; Carl Zeiss, Inc.). To assess macrophage infiltration, frozen cross-sections of TA muscles (16 μm) were labeled with antibodies to CD68 (FA-11, Macrosialin, MCA 1957, AbD Serotec), as described (19). The number of macrophages per square millimeter of cross-sectional area was calculated

by averaging the number of macrophages across eight unique visual fields (40×/1.4 N.A. Plan-Apo objective, Zeiss LSM510) and then by multiplying by a conversion factor (19.75) based on the area of each visual field.

Assessment of Myogenesis 14 d After LSI in Animals Treated with DTZ or PBS. Standard H&E staining was performed on cross-sections of the injured and uninjured TA muscles. Digital images were taken of 10 nonoverlapping fields at 20× magnification, and centrally nucleated fibers (a marker of myofiber degeneration and subsequent regeneration) were counted and expressed as a percentage of the total number of fibers in each field. About 1,000 fibers were counted per injured and uninjured TA muscle. Statistical analyses were performed on the combined data from both animals in each group (diltiazem versus PBS).

Statistical Analyses. Quantitative data were analyzed using GraphPad Prism 5 software (GraphPad Software, Inc.) and are expressed as means ± SEM. Data expressed as percentages were transformed before analysis. Unless otherwise noted, statistically significant differences (set a priori to $P < 0.05$) between groups were assessed by one-way ANOVA or Student t test, as appropriate. Post hoc analyses were performed using the Newman–Keuls method.

ACKNOWLEDGMENTS. We thank W. Jonathan Lederer and Brian M. Hagen (University of Maryland School of Medicine, BioMET) for the use of confocal microscopy facilities and expertise. Dr. Gero Miesenbock (University of Oxford) provided the pHluorin construct. These studies were supported by the Jain Foundation (R.J.B., J.A.R., and S.S.V.) and the Muscular Dystrophy Association (R.J.B.). S.S.V. was supported by the Division of Intramural Clinical and Biological Research of the National Institute on Alcohol Abuse and Alcoholism. A.P.Z. was supported by a Kirschstein–National Research Service Award Individual Postdoctoral Fellowship (F32 AR057647). J.P.K. was supported through the Training Program in Cellular and Integrative Neuroscience (T32 NS007375) and the Interdisciplinary Training Program in Muscle Biology (T32 AR07592).

1. Barohn RJ, Miller RG, Griggs RC (1991) Autosomal recessive distal dystrophy. *Neurology* 41(9):1365–1370.
2. Bansal D, Campbell KP (2004) Dysferlin and the plasma membrane repair in muscular dystrophy. *Trends Cell Biol* 14(4):206–213.
3. Bansal D, et al. (2003) Defective membrane repair in dysferlin-deficient muscular dystrophy. *Nature* 423(6936):168–172.
4. Lennon NJ, et al. (2003) Dysferlin interacts with annexins A1 and A2 and mediates sarcolemmal wound-healing. *J Biol Chem* 278(50):50466–50473.
5. Azakir BA, Di Fulvio S, Therrien C, Sinnreich M (2010) Dysferlin interacts with tubulin and microtubules in mouse skeletal muscle. *PLoS ONE* 5(4):e10122.
6. Di Fulvio S, Azakir BA, Therrien C, Sinnreich M (2011) Dysferlin interacts with histone deacetylase 6 and increases alpha-tubulin acetylation. *PLoS ONE* 6(12):e28563.
7. de Morrée A, et al. (2013) Dysferlin regulates cell adhesion in human monocytes. *J Biol Chem* 288(20):14147–14157.
8. Sharma A, et al. (2010) A new role for the muscle repair protein dysferlin in endothelial cell adhesion and angiogenesis. *Arterioscler Thromb Vasc Biol* 30(11): 2196–2204.
9. Covian-Nares JF, Koushik SV, Puhl HL, III, Vogel SS (2010) Membrane wounding triggers ATP release and dysferlin-mediated intercellular calcium signaling. *J Cell Sci* 123(Pt 11):1884–1893.
10. Roche JA, et al. (2011) Unmasking potential intracellular roles for dysferlin through improved immunolabeling methods. *J Histochem Cytochem* 59(11):964–975.
11. Ampong BN, Imamura M, Matsumiya T, Yoshida M, Takeda S (2005) Intracellular localization of dysferlin and its association with the dihydropyridine receptor. *Acta Myol* 24(2):134–144.
12. Matsuda C, et al. (2001) The sarcolemmal proteins dysferlin and caveolin-3 interact in skeletal muscle. *Hum Mol Genet* 10(17):1761–1766.
13. de Morrée A, et al. (2010) Proteomic analysis of the dysferlin protein complex unveils its importance for sarcolemmal maintenance and integrity. *PLoS ONE* 5(11):e13854.
14. Waddell LB, et al. (2011) Dysferlin, annexin A1, and mitsugumin 53 are upregulated in muscular dystrophy and localize to longitudinal tubules of the T-system with stretch. *J Neuropathol Exp Neurol* 70(4):302–313.
15. Klinge L, et al. (2010) Dysferlin associates with the developing T-tubule system in rodent and human skeletal muscle. *Muscle Nerve* 41(2):166–173.
16. Terrill JR, et al. (2013) Oxidative stress and pathology in muscular dystrophies: Focus on protein thiol oxidation and dysferlinopathies. *FEBS J* 280(17):4149–4164.
17. Kobayashi K, Izawa T, Kuwamura M, Yamate J (2011) Comparative gene expression analysis in the skeletal muscles of dysferlin-deficient SJL/J and A/J mice. *J Toxicol Pathol* 24(1):49–62.
18. Roche JA, Ru LW, Bloch RJ (2012) Distinct effects of contraction-induced injury in vivo on four different murine models of dysferlinopathy. *J Biomed Biotechnol* 2012: 134031.
19. Roche JA, et al. (2010) Extensive mononuclear infiltration and myogenesis characterize recovery of dysferlin-null skeletal muscle from contraction-induced injuries. *Am J Physiol Cell Physiol* 298(2):C298–C312.
20. Roche JA, Lovering RM, Bloch RJ (2008) Impaired recovery of dysferlin-null skeletal muscle after contraction-induced injury in vivo. *Neuroreport* 19(16):1579–1584.
21. Miesenböck G, De Angelis DA, Rothman JE (1998) Visualizing secretion and synaptic transmission with pH-sensitive green fluorescent proteins. *Nature* 394(6689):192–195.
22. Menke A, Jockusch H (1991) Decreased osmotic stability of dystrophin-less muscle cells from the mdx mouse. *Nature* 349(6304):69–71.
23. Martins AS, Shkryl VM, Nowycky MC, Shirokova N (2008) Reactive oxygen species contribute to Ca2+ signals produced by osmotic stress in mouse skeletal muscle fibres. *J Physiol* 586(1):197–210.
24. Shkryl VM, et al. (2009) Reciprocal amplification of ROS and Ca($^{2+}$) signals in stressed mdx dystrophic skeletal muscle fibers. *Pflugers Arch* 458(5):915–928.
25. Pickering JD, White E, Duke AM, Steele DS (2009) DHPR activation underlies SR Ca2+ release induced by osmotic stress in isolated rat skeletal muscle fibers. *J Gen Physiol* 133(5):511–524.
26. Friedrich O, Both M, Gillis JM, Chamberlain JS, Fink RH (2004) Mini-dystrophin restores L-type calcium currents in skeletal muscle of transgenic mdx mice. *J Physiol* 555(Pt 1): 251–265.
27. Hornsey MA, Laval SH, Barresi R, Lochmüller H, Bushby K (2013) Muscular dystrophy in dysferlin-deficient mouse models. *Neuromuscul Disord* 23(5):377–387.
28. Gallardo E, et al. (2001) Inflammation in dysferlin myopathy: immunohistochemical characterization of 13 patients. *Neurology* 57(11):2136–2138.
29. Rawat R, et al. (2010) Inflammasome up-regulation and activation in dysferlin-deficient skeletal muscle. *Am J Pathol* 176(6):2891–2900.
30. Anderson LV, et al. (1999) Dysferlin is a plasma membrane protein and is expressed early in human development. *Hum Mol Genet* 8(5):855–861.
31. Matsuda C, et al. (1999) Dysferlin is a surface membrane-associated protein that is absent in Miyoshi myopathy. *Neurology* 53(5):1119–1122.
32. Han R, Rader EP, Levy JR, Bansal D, Campbell KP (2011) Dystrophin deficiency exacerbates skeletal muscle pathology in dysferlin-null mice. *Skelet Muscle* 1(1):35.
33. Han R, et al. (2010) Genetic ablation of complement C3 attenuates muscle pathology in dysferlin-deficient mice. *J Clin Invest* 120(12):4366–4374.
34. Azakir BA, et al. (2012) Modular dispensability of dysferlin C2 domains reveals rational design for mini-dysferlin molecules. *J Biol Chem* 287(33):27629–27636.
35. Han WQ, et al. (2012) Lysosome fusion to the cell membrane is mediated by the dysferlin C2A domain in coronary arterial endothelial cells. *J Cell Sci* 125(Pt 5): 1225–1234.
36. Cenacchi G, Fanin M, De Giorgi LB, Angelini C (2005) Ultrastructural changes in dysferlinopathy support defective membrane repair mechanism. *J Clin Pathol* 58(2): 190–195.
37. Krahn M, et al. (2010) A naturally occurring human minidysferlin protein repairs sarcolemmal lesions in a mouse model of dysferlinopathy. *Sci Transl Med* 2(50): 50ra69.
38. Lostal W, et al. (2010) Efficient recovery of dysferlin deficiency by dual adeno-associated vector-mediated gene transfer. *Hum Mol Genet* 19(10):1897–1907.
39. Lostal W, et al. (2012) Lack of correlation between outcomes of membrane repair assay and correction of dystrophic changes in experimental therapeutic strategy in dysferlinopathy. *PLoS ONE* 7(5):e38036.
40. Cai C, et al. (2009) Membrane repair defects in muscular dystrophy are linked to altered interaction between MG53, caveolin-3, and dysferlin. *J Biol Chem* 284(23): 15894–15902.
41. Cai C, et al. (2009) MG53 nucleates assembly of cell membrane repair machinery. *Nat Cell Biol* 11(1):56–64.
42. Dirksen RT (2009) Checking your SOCCs and feet: The molecular mechanisms of Ca2+ entry in skeletal muscle. *J Physiol* 587(Pt 13):3139–3147.
43. Lovering RM, Roche JA, Goodall MH, Clark BB, McMillan A (2011) An in vivo rodent model of contraction-induced injury and non-invasive monitoring of recovery. *J Vis Exp* (51), pii: 2782.
44. Ingalls CP, Warren GL, Zhang JZ, Hamilton SL, Armstrong RB (2004) Dihydropyridine and ryanodine receptor binding after eccentric contractions in mouse skeletal muscle. *J Appl Physiol (1985)* 96(5):1619–1625.
45. Brown LD, Rodney GG, Hernández-Ochoa E, Ward CW, Schneider MF (2007) Ca2+ sparks and T tubule reorganization in dedifferentiating adult mouse skeletal muscle fibers. *Am J Physiol Cell Physiol* 292(3):C1156–C1166.
46. Bolte S, Cordelières FP (2006) A guided tour into subcellular colocalization analysis in light microscopy. *J Microsc* 224(Pt 3):213–232.
47. DiFranco M, Quinonez M, Capote J, Vergara J (2009) DNA transfection of mammalian skeletal muscles using in vivo electroporation. *J Vis Exp* (32), pii: 1520.
48. Yeung EW, Balnave CD, Ballard HJ, Bourreau JP, Allen DG (2002) Development of T-tubular vacuoles in eccentrically damaged mouse muscle fibres. *J Physiol* 540(Pt 2): 581–592.
49. Lovering RM, Michaelson L, Ward CW (2009) Malformed mdx myofibers have normal cytoskeletal architecture yet altered EC coupling and stress-induced Ca2+ signaling. *Am J Physiol Cell Physiol* 297(3):C571–C580.
50. Goodall MH, Ward CW, Pratt SJ, Bloch RJ, Lovering RM (2012) Structural and functional evaluation of branched myofibers lacking intermediate filaments. *Am J Physiol Cell Physiol* 303(2):C224–C232.
51. Matsumura CY, Pertille A, Albuquerque TC, Santo Neto H, Marques MJ (2009) Diltiazem and verapamil protect dystrophin-deficient muscle fibers of MDX mice from degeneration: A potential role in calcium buffering and sarcolemmal stability. *Muscle Nerve* 39(2):167–176.